Article

On the Mechanism of a No-metal-added Heterocycloisomerization of Alkynylcyclopropylhydrazones: A Synthesis of Cycloheptane-fused Aminopyrroles Facilitated by Copper Salts at Trace Loadings.

Sidney M. Wilkerson-Hill, Diana Yu, Phillip P. Painter, Ethan L. Fisher, Dean J Tantillo, Richmond Sarpong, and Jason E Hein

J. Am. Chem. Soc., **Just Accepted Manuscript** • DOI: 10.1021/jacs.7b06007 • Publication Date (Web): 06 Jul 2017

On the Mechanism of a No-metal-added Heterocycloisomerization of Alkynylcyclopropylhydrazones: A Synthesis of Cycloheptane-fused Aminopyrroles Facilitated by Copper Salts at Trace Loadings

Sidney M. Wilkerson-Hill,[1] † Diana Yu,[2] †† Phillip P. Painter,[3] Ethan L. Fisher,[1] ††† Dean J. Tantillo,[3]* Richmond Sarpong[1]*and Jason E. Hein[2]*††.

[1] Department of Chemistry, University of California, Berkeley, CA 94720, United States.

[2] Chemistry and Chemical Biology, University of California, Merced, CA 95343, United States.

[3] Department of Chemistry, University of California, Davis, CA 95616, United States.

ABSTRACT: A mechanistic study of a new heterocycloisomerization reaction that forms annulated aminopyrroles is presented. Density functional theory (DFT) calculations and kinetic studies suggest the reaction is catalyzed by trace copper salts and that a *Z*- to *E*-hydrazone isomerization occurs through an enehydrazine intermediate before the rate-determining cyclization of the hydrazone onto the alkyne group. The aminopyrrole products are obtained in 36–93% isolated yield depending on the nature of the alkynyl substituent. A new automated sampling technique was developed to obtain robust mechanistic data.

INTRODUCTION

High turnover catalysis (HTC), defined as catalysis using transition metal complexes at 0.1 mol% or lower loading and leading to quantitative conversion of starting materials, has surfaced in recent years as an extremely powerful and environmentally benign form of transition metal catalysis.[1–4] However, 'accidental' HTC has also beset researchers when trying to develop mechanistic understanding of certain reactions, as sometimes reaction milieu contain trace impurities that facilitate catalysis with very high turnover number (TON). Studies by Leadbeater and Marco on "transition metal-free" Suzuki cross-couplings in water, for example, were shown to be catalyzed by trace palladium impurities found in the sodium carbonate used for the reaction.[5a] Likewise, amination reactions studied by Bolm that were thought to be mediated by iron salts, were in fact catalyzed by trace copper impurities at the parts-per-million level (Figure 1, A).[5b] These studies attest to the significant challenge of identifying the true active catalyst in cross-coupling reactions and serve as a starting point for developing a mechanistic understanding of other metal-catalyzed, and "metal-free" processes.

Over the last decade, transition metal-catalyzed cycloisomerization reactions involving alkyne substrates that rely on the use of 'soft' π-Lewis acid catalysts have emerged.[6–9] These reactions are attractive synthetically because, ideally, all of the starting material is converted to the product without the formation of byproducts.[10,11] The underlying tenet for successful application of π-Lewis acid metal salts as catalysts in these reactions is that highly favorable interactions between the alkyne group and metal center serve to initiate the cycloisomerization process. For many of these reactions, substantial rate accelerations are observed compared to the uncatalyzed process, and the course of the reaction is heavily influenced by the choice of metal or ligands on the active catalyst complex. The Sarpong laboratory[12] and others[13] have described the promotion of heterocycloisomerization reactions that had been previously conducted using π-phillic transition metal catalysts by barrier-lowering hydrogen bonding networks.[14] For example, several transition metal salts and complexes based on Pt, Cu or Ag had been reported to facilitate the heterocycloisomerization reaction to form indolizine **8** (Figure 1, B) from **7**. The Sarpong group found that the transformation proceeds simply by heating in water (or MeOH) and, importantly, proceeds in an appreciably higher yield (compared to the $PtCl_2$-catalyzed example) (Figure 1, B). However, detailed mechanistic studies of these metal-free reactions have not been performed, and so the possibility of trace levels of transition metals facilitating this class of reactions cannot be excluded.

Herein, we report our detailed mechanistic investigation of a newly discovered "no-metal-added" variant of chemistry reported by Schmalz and Zhang[15] (Figure 1, C) using density functional theory (DFT) calculations and *in situ* monitoring of the reaction using an automated sampling approach. We demonstrate that the reaction is not metal-free and is catalyzed by trace copper salts at very low catalyst loadings. Importantly, our understanding of the chemical reactivity observed hinged on the combination of a diverse array of tools and techniques, ranging from analytical instrumentation to computational and experimental evaluation of model systems.[16]

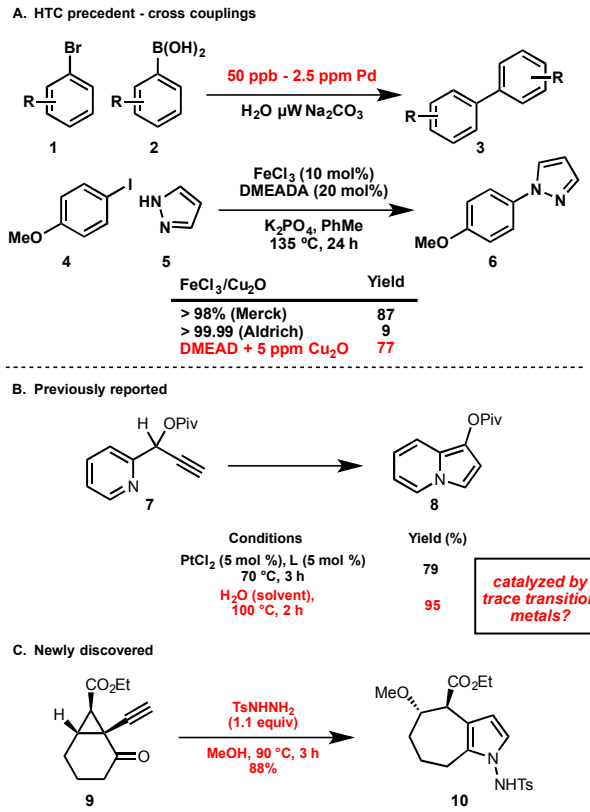

Figure 1: A) Trace metal catalysis in cross-coupling chemistry. B) Previously reported metal-free cycloisomerization reaction C) Newly developed cycloisomerization reaction.

DEUTERIUM LABELING AND COMPUTATIONAL STUDIES.

The initial discovery of the ring-expansion/cycloisomerization reaction (Figure 1, C) led to a key question; why does this reaction proceed with high efficiency solely through thermal activation in methanol? To investigate the origin of alkyne activation by the protic solvent, we began to explore the reaction mechanism and initially proposed the straightforward reaction pathway outlined in Scheme 1. Condensation of ketone **9** with *para*-toluenesulfonyl hydrazide (PTSH) was expected to give a mixture of *E*- and *Z*- hydrazones **11**. While it is likely that only the *E*-hydrazone would possess the required geometry for productive cycloisomerization, the two isomers could readily equilibrate through enehydrazine **12**.[17] Pyrrole ring formation would then occur via intramolecular 5-*endo*-dig cyclization, giving tricyclic iminium ion intermediate **13**. Nucleophilic addition of methanol at this stage would proceed with rupture of the endocyclic cyclopropane C–C bond and concomitant aromatization of the pyrrole, furnishing bicyclic *N*-aminopyrrole **10**.

This pathway requires appropriate activation of *E*-hydrazone **11** to facilitate ring closure. Our initial hypothesis was that a Brønsted acid would provide the necessary activation of the alkyne, possibly benefiting from assistance from the proximal ester group. The most likely source of the needed acid activator would be sulfinic acid, generated *in situ* from thermal decomposition of tosyl hydrazide to liberate the acid and diimide (Scheme 1, Step 1). This proposal aligned well with preliminary results, accounting for the required elevated temperature that would generate the Brønsted acid prior to the onset of cycloisomerization. Notably, productive cycloisomerization was only observed when a slight excess of PTSH was used, again in line with the proposed mode of activation.[2]

We hypothesized that if this unique mode of alkyne activation was in fact operational, the reaction rate should display a significant kinetic isotope effect. Thus, we undertook a series of deuterium labeling experiments.

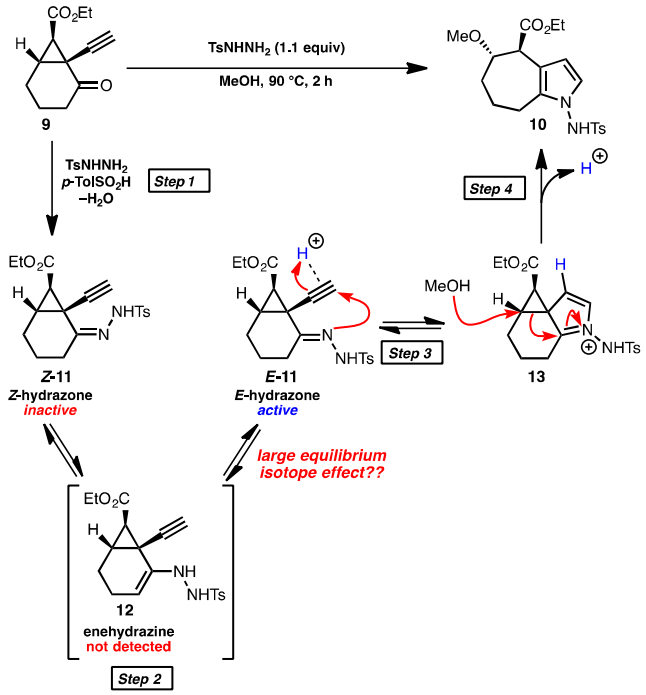

Scheme 1: Initially proposed heterocycloisomerization mechanism under metal free conditions.

First, upon treatment of ketone **9** with $TsNDND_2$ in CD_3OD, deuteration at C(3) (90% D) was observed along with the addition of the CD_3OD group (see Eq. 1, Figure 2) as anticipated. Deuteration at C(2) (97% D) and, surprisingly, at C(8) (99% D) was also observed. Next, examining the reaction at several time points allowed us to explain the likely origins of each H/D exchange event. At low conversion (*ca.* 20%), ^1H NMR analysis of the product revealed 88% deuterium incorporation at C(3) and only 42% D at C(2), which increased to 97% over 2 h. At this early time point, the product also displays 99% deuterium incorporation at C(8), suggesting that the pre-equilibrium between the *E*- and *Z*-hydrazone **11** via enhydrazine **12** is quite facile, resulting in C(8) deuteration. We independently confirmed that C(8) deuteration precedes cycloisomerization by reacting ketone **9** with $TsNDND_2$ at 45 ºC. This treatment gave **11** as a mixture of *E*- and *Z*-isomers, both displaying > 95% C(8) deuterium incorporation without giving significant cycloisomerization product **10**. Furthermore, heating the isolated product at 90 ºC in CD_3OD also led to > 95% deuteration at C(2) and C(3), indicating that H/D exchange at these positons was likely occurring via electrophilic aromatic substitution (Eq. 2, Figure 2). In this experiment, no deuterium incorporation was observed at C(8).

In addition to observations relating to the regioselectivity of deuterium incorporation, these experiments revealed that the overall rate of reaction was significantly affected by deuterium incorporation. Specifically, performing the reaction with d_2-**9**,

which was prepared by H/D exchange from **9** in EtOD using base, led to a dramatically reduced rate of cycloisomerization, with only 17% conversion to product after 2 h under normal reaction conditions (Eq. 3, Figure 2). This preliminary result was striking, as the reaction appeared to display an abnormally large KIE of 24 when C(8) of ketone **9** was fully deuterated.[18] Furthermore, this result was notable considering the rate of the reaction in Eq. 1 was not affected by deuteration, even though we demonstrated that deuteration of hydrazone intermediates occurs under the reaction conditions and precedes cyclization. Thus, we ascertained that other factors were at play and hypothesized that the effect could possibly be explained by invoking a rate limiting pre-equilibrium of *Z*-hydrazone **11** to *E*-hydrazone **11** (*i.e.,* α-deprotonation of the *Z*-hydrazone **11** is required to access the *E*-hydrazone which then undergoes the 5-*exo*-dig cyclization).

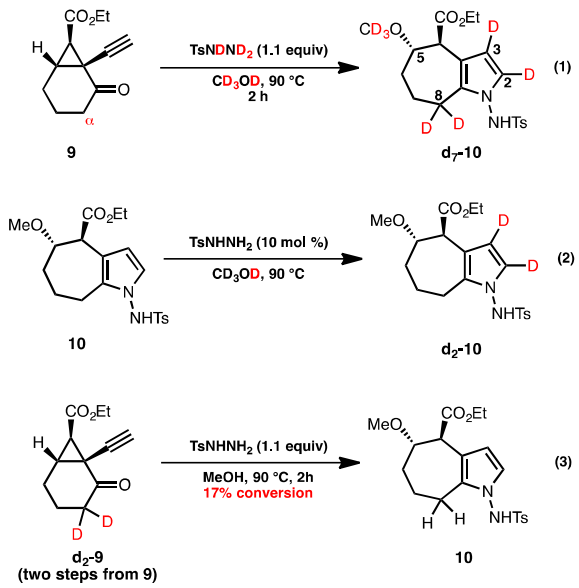

Figure 2: Deuterium labeling studies using ketone **9**, aminopyrrole **10** and ketone **d_2-9**.

The ring-expansion/cycloisomerization reaction was also examined using quantum chemical computations. Our initial calculations were aimed at finding an energetically viable mechanism that was consistent with the observed isotope effect data. We employed a model system in which the tosyl and ethyl groups of the substrate were truncated to mesyl and methyl groups for computational efficiency, and explicit methanol and CH_3SO_2H molecules were included. The M06-2X/6-31+G(d,p) DFT method,[19] as implemented in GAUSSIAN09,[20] was used, along with the SMD continuum solvation model[21] for methanol at 365 K.[22, 23]

Consistent with the experimental results described above, our calculations indeed predict that the *Z*-hydrazone (Figure 3, *Z*-**A**) is lower in energy than the *E*-hydrazone (Figure 3, *E*-**A**)), by almost 2 kcal/mol. Furthermore, direct interconversion of the two hydrazones via a linear C=N-NR geometry is predicted to have a barrier of 27 kcal/mol. Ring closure from the *E*-hydrazone via transition state structure $\mathbf{TS_{AC}}$ (activation of the alkyne with sulfinic acid) is associated with a barrier (versus *Z*-hydrazone) of 29 kcal/mol. Subsequent capture by methanol (via $\mathbf{TS_{CD}}$) is predicted to be facile. These calculations suggest that the ring closure step is rate-determining, yet deuteration of the α-position in such a scenario would result in a secondary inverse effect (supported by DFT predictions; see the Supporting Information),[24] as opposed to the observed apparent primary effect. Enamine formation was also considered (Figure 3, left), but ring-closure from an enamine intermediate is predicted to have a prohibitively high barrier (>40 kcal/mol), due in part to the poor nucleophilicity of the enamine nitrogen associated with loss of conjugation upon attack. These results left us at a loss for understanding the 'kinetic isotope effect' observed for the reaction in Eq 3.

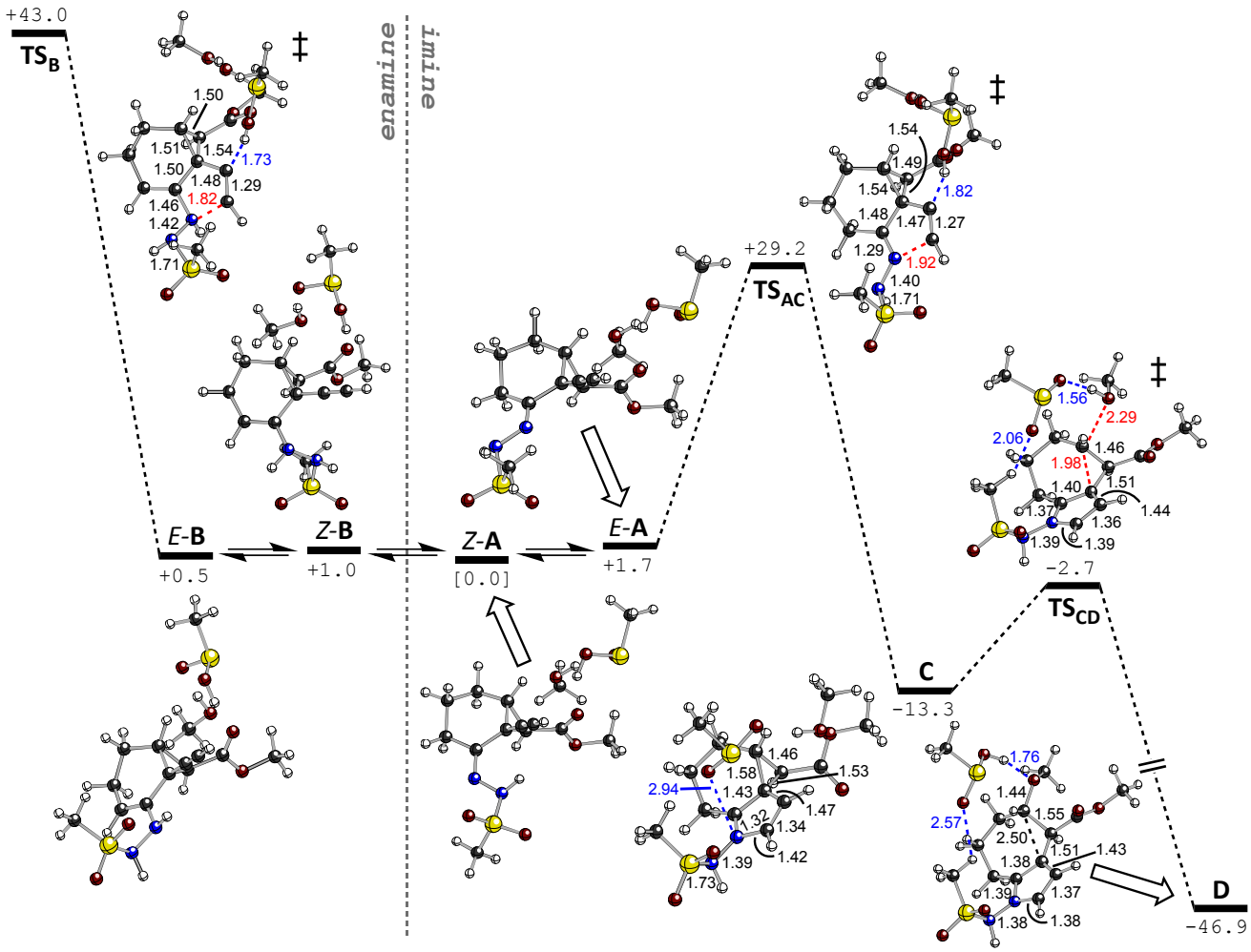

Figure 3: Optimized structures (SMD(methanol)-M06-2X/6-31+G(d,p)) for metal-free cyclization pathways. Relative free energies are shown in kcal/mol and selected distances are shown in Å.

IN SITU MECHANISTIC STUDIES

With these computational results in hand, we then sought to conclusively exclude the possibility that the large effect of α-deuteration on the rate of the reaction using ketone **9** was not due to a rate-determining pre-equilibrium of hydrazone *Z*-**11** to *E*-**11** (Scheme 1). Furthermore, we sought to rule out the possibility that the sulfinic acid, generated from the thermal decomposition of *p*-$TsNHNH_2$,[25] was serving as the active catalyst for this reaction. As such we turned to monitoring the reaction by React-IR and LCMS. Monitoring this reaction, which proceeds above the boiling point of methanol, was not trivial and required the development of a new apparatus (see Figure 4).

While DFT and deuteration analysis of individual reaction aliquots each provided some clues, monitoring the dynamic reaction progress was necessary to elucidate the underlying mechanism of this reaction. Delineation of a mechanism using this approach requires time-dependent concentration data for all species, over the entire course of the reaction, ideally with a very high data sampling rate. Techniques such as NMR[26] and ReactIR[27] are excellent candidates for monitoring reactions in real time, but the required temperature and pressure (superheated MeOH at 90 ºC) and the lack of discrete diagnostic spectroscopic signals complicated our ability to apply those technologies.

Instead, we developed an automated reaction sampling apparatus, consisting of a programmable syringe pump, a high-torque 2-position - 6 port Rheodyne® valve and a Gilson 215 liquid handling robot.[28] An example of the workflow for capturing each aliquot is illustrated in Figure 4. The reaction is initiated by adding the reagents, stir bar, and solvent. The vessel is then sealed in a vial using a PTFE-lined septum with a 1/32" micro capillary threaded through to act as a sampling port. The reaction vial is then immersed in an aluminum block fitted into a EasyMax reactor preheated to 90 ºC. At the start of the sampling sequence, the Rheodyne® value rotates to bring a sample loop in line with the micro-capillary, and the syringe pump withdraws a fixed volume (~5-10 µL) from the reactor. The combination of overpressure in the reaction flask and a predetermined draw rate ensures an accurate volume is transferred to the sample loop, without cavitation of the solvent. The Rheodyne® valve then switches, and the liquid handler actuates, flushing the contents of the sample loop into an HPLC vial. This sampling protocol proved to be highly repro-

ducible, allowing reaction profiles to be easily generated from complex reaction mixtures.

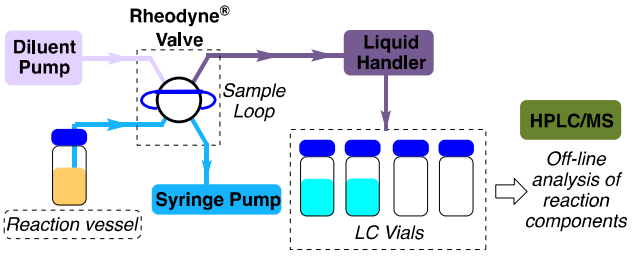

Figure 4: Representation of work flow for automated sampling with offline HPLC-MS analysis apparatus.

Applying our automated sampling apparatus permits rapid, detailed analysis of the reaction components. In a preliminary survey, we were able to immediately identify several reaction trends, which support our proposed reaction pathway (Figure 5). Within the first 60 minutes we observed rapid formation of two isomeric hydrazones (*Z*-**11** and *E*-**11**), with maximum concentration achieved at ~50 minutes. Only after these intermediates are generated is the desired amino pyrrole **10** observed. The induction period most likely reflects the need for sufficient *E*-hydrazone prior to cycloisomerization, however, it could also be due to slow *in situ* generation of the necessary sulfinic acid catalyst.

The reaction progress information compelled us to prepare authentic samples of each hydrazone, unambiguously establishing the configuration of each isomer by X-ray crystallography from individual samples (Figure 6). These data allow us to conclusively show that the system does indeed form both

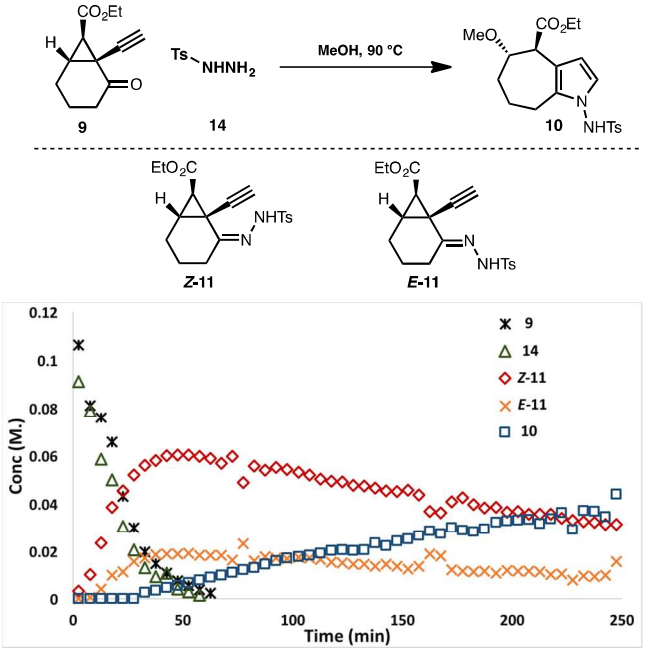

Figure 5: Reaction profile for ketone **9** heterocycloisomerization obtained by automated sampling and analysis by HPLC-MS.

hydrazones, with a 3:1 ratio favoring the unreactive *Z*-isomer, which is in good agreement with our DFT analysis.

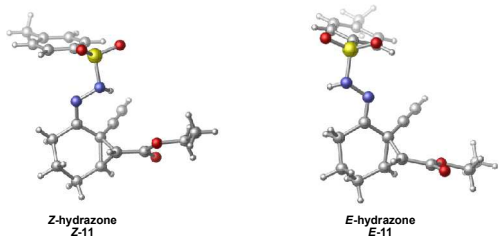

Figure 6: X-ray crystal structures of *E*- and *Z*- hydrazone **11**.[29]

The ability to visualize the dynamic behavior of multiple intermediates, products and byproducts allowed us to directly test our mechanistic hypothesis. We surmised that if in situ generated sulfinic acid was indeed the active catalyst the rate of pyrrole formation should increase with higher initial loadings of $TsNHNH_2$ (**14**), as we would expect higher concentrations of the putative Brønsted acid catalyst.[25] Instead, increasing the initial concentration of $TsNHNH_2$ resulted in slower formation of pyrrole, with a concomitant increase in alkane byproduct **15**, which arises from diimide reduction of the alkyne group in *Z*-hydrazone **11**. While this result transitively confirms elevated thermal decomposition of $TsNHNH_2$, the lack of more rapid pyrrole formation suggests that if sulfinic acid is indeed a Brønsted acid catalyst, the reaction rate is not sensitive to its concentration, implying that either the system displays saturation kinetics relative to sulfinic acid or that it is not participating in the cycloisomerization pathway (Figure 7).

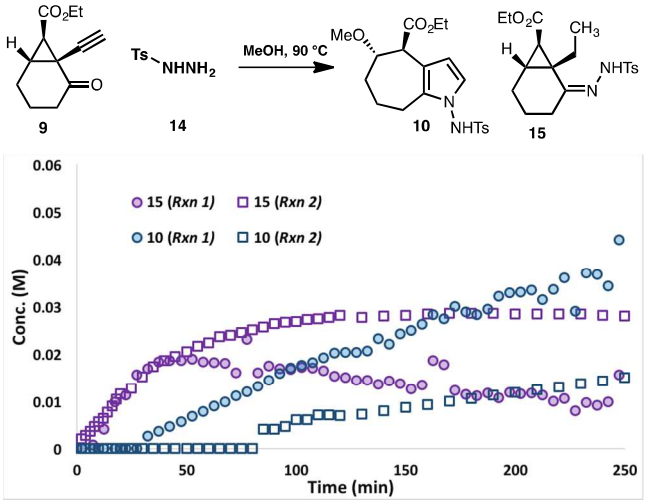

Figure 7: Changes in chemoselectivity with varied initial loading of $TsNHNH_2$, Rxn 1 = [$TsNHNH_2$] = 0.35 M, [ketone **9**] = 0.25 M, Rxn 2 = [$TsNHNH_2$] = 0.55 M, [ketone **9**] = 0.25 M.

Following this observation, we discovered that the rate of pyrrole formation varies with the manner in which ketone **9** is purified. The rate of aminopyrrole **10** formation was significantly faster when using ketone **9** that was purified by column chromatography compared to ketone **9** that was purified by recrystallization from EtOH. Furthermore, a rapid rate of cyclization could be restored if an aliquot of the filtrate was added to the cycloisomerization reaction using recrystallized ketone **9** (Figure **8**). Finally, the rate of ketone consumption to form *Z*- and *E*-hydrazones is identical regardless of how the reaction is performed (green line in graph). These results suggest that a trace catalyst exists in the sample that is not effec-

tively removed by column chromatography and specifically accelerates the cyclization from the intermediate hydrazone without impacting the condensation or hydrazone equilibration steps.

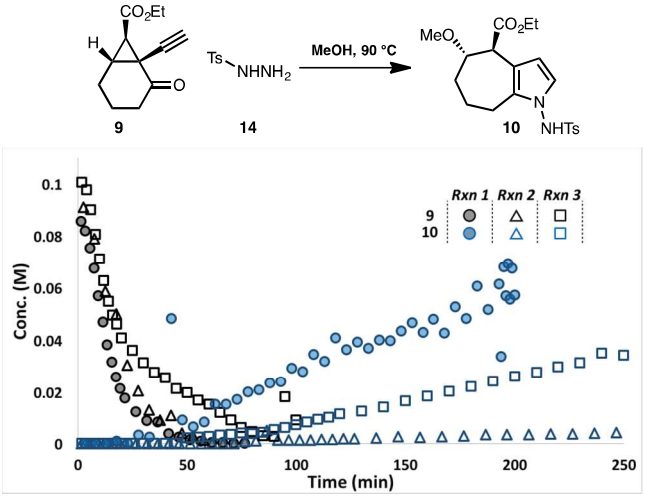

Figure 8: Rate of cycloisomerization varies with purification method utilized for ketone **9**. General reaction conditions [ketone **9**] = 0.1 M, [$TsNHNH_2$] = 0.11 M in MeOH at 95 °C; Rxn 1 – Ketone **9** purified by column chromatography; Rxn 2 – ketone **9** purified by recrystallization from EtOH; Rxn 3 – Recrystallized ketone **9** was treated with 5 µL of concentrated filtrate from recrystallization.

To identify the nature of the trace catalyst present in the sample, ICP-MS analysis was conducted on both the column-purified and recrystallized ketone, as well as the supernatant from the crystallization. While many trace metals were present, the key difference between the samples is a depletion of copper upon recrystallization from EtOH. In addition, there is a concomitant increase of copper in the supernatant (Table 1).

The trace copper contamination likely results from the Sonogashira cross-coupling, used to install the alkyne functional group in ketone **9**.[15] It is quite remarkable that a catalytically sufficient quantity of copper remains in **9**, even after three synthetic steps, each using purification by standard techniques (column chromatography or extraction). Furthermore, this result also illustrates the extraordinary catalytic efficiency of copper, which is able to promote the cycloisomerization reaction at a loading of nearly 2.0 x 10^{-5} mol equiv (TON ≈ 50000).

Table 1: Comparison of Cu levels in starting material after purifications.

Entry	Sample	%Cu (mg/mg)[a]	Equiv Cu[b]
1	**9** (chromatography)	2.76 x 10^{-2}	9.01 x 10^{-4}
2	**9** (recrystallized)	6.40 x 10^{-4}	2.09 x 10^{-5}
3	supernatant	1.17 x 10^{-1}	3.79 x 10^{-3}

[a] percent Cu by mass expressed in mg Cu per mg total sample; [b] calculated equivalents of Cu present in cycloisomerization reaction, relative to ketone **9**.

Initial experiments had flagged the apparent differences in rate between **9** and d_2-**9** as having key mechanistic implications, however, the realization that trace copper salts are key to catalysis forced us to reexamine the role of α-deuteration. Especially because our detailed computational investigation could provide no rationale for the observed differences in reaction rate depending on deuterium incorporation at the α-position of **9**.

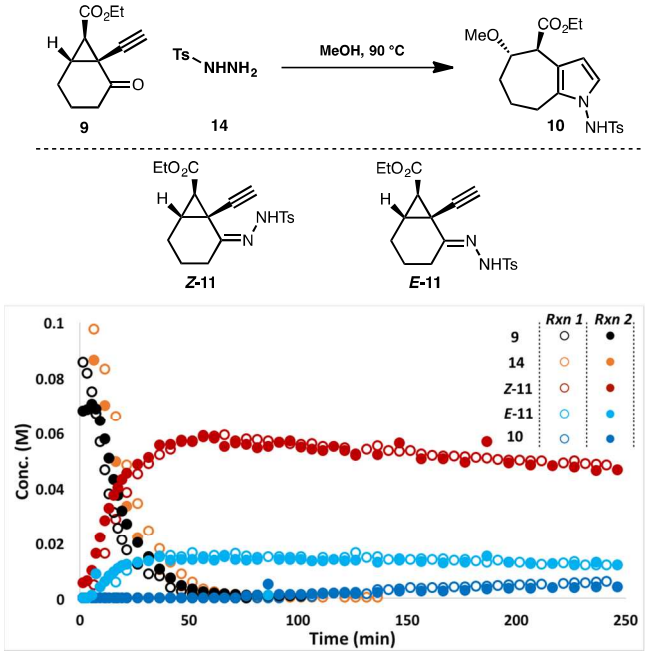

Figure 9: Cycloisomerization reaction initiated using either C(8)-H_2 or C(8)-d_2 ketone (both recrystallized from EtOH). Initial conditions - Rxn 1: [ketone **9**] = 0.1 M, [hydrazide **14**] = 0.11 M in MeOH at 95 °C; Rxn 2: [ketone d_2-**9**] = 0.1 M, [hydrazide **14**] = 0.11 M in MeOH at 95 °C.

After recrystallizing ketone **9** and d_2-**9** from EtOH, both starting materials were independently subjected to the reaction conditions. Now, both the α-protio and α-deutero ketones produced nearly identical reaction progress curves (Figure 9). Thus, our initially observed reduction in cycloisomerization rate upon α-deuteration is simply due to the synthetic operations used to make **d_2-9**, not the deuterium isotope itself. To obtain d_2-**9**, ketone **9** was dissolved in EtOD under basic conditions. Reaction and isolation lowers the concentration of copper sufficiently, such that the rate of cyclization was seriously hindered for d_2-**9**; recrystallization of ketone **9** also serves a similar purpose.

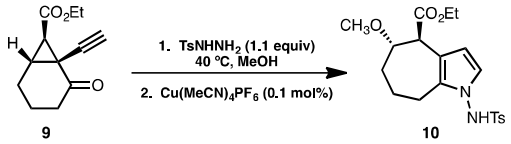

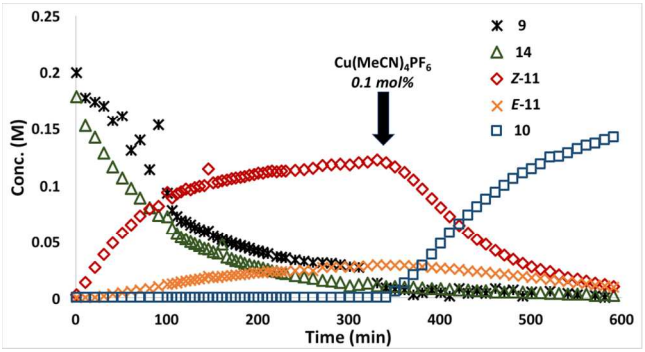

Figure 10: Cycloisomerization initiated by $Cu(MeCN)_4PF_6$ addition. General reaction conditions [ketone **9**] = 0.2 M, [$TsNHNH_2$] = 0.2 M in MeOH at 45 °C. [$Cu(MeCN)_4PF_6$] = 0.2 μM added at indicated time.

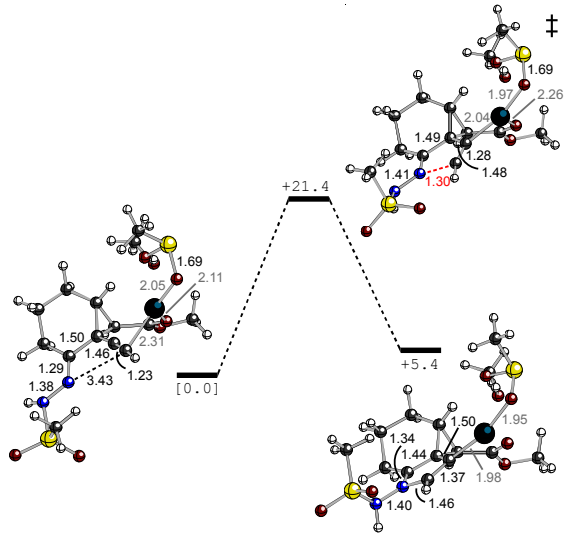

Figure 11: Optimized structures (M06-2X/LANL2DZ) for Cu-promoted cyclization. Relative free energies are shown in kcal/mol and selected distances are shown in Å.

Copper salts were confirmed to be a very effective catalyst by performing the reaction with $Cu(MeCN)_4PF_6$. In this experiment, recrystallized **9** and **14** were incubated in MeOH at 40 °C until all ketone was converted to hydrazone **11** (Figure 10). The $Cu(MeCN)_4PF_6$ (0.1 mol%) was then added, resulting in rapid cycloisomerization. Additional calculations with copper (modeled here as $Cu(CH_3SO_2)$) were performed using the M06-2X/LANL2DZ model chemistry[30] to confirm that Cu(I) does lead to barrier lowering. Our results (Figure 11) indicate that ring-closure from the *E*-hydrazone does indeed have a reduced (by ~6 kcal/mol) barrier when the copper salt complexes to the alkyne π-bond, as expected.

SUBSTRATE SCOPE

As illustrated in Figure 12, this HTC hydrazone variant of the Schmalz-Zhang transformation works for a range of internal alkyne-bearing substrates. The key difference between the terminal alkyne case and the internal alkyne cases is that in the latter, mixtures of diastereomeric products are observed. Aryl substitution on the alkyne unit is readily tolerated as evidenced by the formation of **10a**–**10f**. A cyclopropyl substituent on the alkyne led to the formation of **10g** in 73% yield. Importantly, this reaction proceeded at 75 °C as compared to the 90 °C required for terminal alkyne substrate **9**. Of note, increasing steric bulk by *ortho*-substitution on the aryl group (see **10i**) leads to a lower yield of the desired product. A cyclohexenyl substituent yielded the corresponding vinyl aminopyrrole product (**10j**) in 36% yield. Vinyl pyrroles are known to readily decompose under acidic and aerobic conditions, which likely accounts for the low isolated yield of **10j**.[31] Significantly, none of the desired product was observed for substrates possessing *n*-alkyl substitution on the alkyne group. In these cases (e.g., R = n-Bu or hexyl), only non-specific decomposition occurred upon prolonged heating. Thus, it appears that a balance of stereoelectronic effects is important for these transformations.

MECHANISTIC PROPOSAL

On the basis of the collection of observations described above, along with insights from the analogous gold-catalyzed transformations described by Schmalz and Zhang,[15] a plausible mechanism for the heterocycloisomerization can be formulated as illustrated in Scheme 2, A. Condensation of ketones **9a-k** with $TsNHNH_2$ leads to the formation of hydrazones *E/Z*-**11a-k**. Concurrent thermal decomposition of $TsNHNH_2$ results in the formation of small, but significant, quantities of p-$TolSO_2H$, which possibly facilitates the isomerization of *Z*-hydrazones *Z*-**11a-k** to *E*-hydrazones **11a-k** through an enehydrazine intermediate that is undetected in our kinetic studies but implied from our deuterium labeling experiments (see Figure 2, Eq. 3). Activation of the alkyne group with trace copper salts and attack of the hydrazone imine in a 5-*endo*-dig fashion affords iminium ions **13a-k**. The addition of methanol to **13a-k** at this stage may proceed with attendant rupture of the endocyclic cyclopropane C–C bond and aromatization to afford bicyclic aminopyrroles **10a-k**.

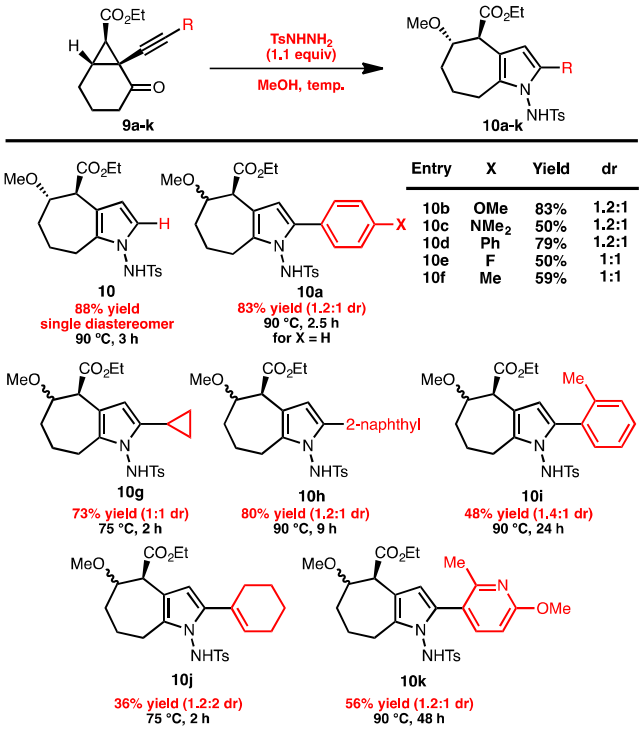

Figure 12: Scope of the HTC-aminopyrrole formation. Unless indicated, the stereochemistry of the major diastereomer was not determined.

Finally, changes in the electronic and steric properties of the alkyne substituent impact both the reactivity and diastereoselectivity of the resulting products. This may be explained by the influence of substituents on Step 3 (see Scheme 2) of our proposed mechanism. As illustrated in Scheme 2, B, groups that are electron-releasing are likely to stabilize cumulene intermediates such as **16**, which would in turn be reflected in a lower associated barrier for the metal coordination step. Furthermore, intramolecular cyclization by the hydrazone group would be hampered by increased steric interaction with the R group, which is reflected in our observations with, for example, *ortho*-substituted phenyl groups (see **10i** and **10k**, Figure 12). Following attack, iminium intermediate **13a-k** is formed. The R group (in the cases where it is electron releasing) could enhance stabilization of cationic intermediate **17** by the aminopyrrole moiety. As a result, the methanol addition step would lead to a cationic intermediate (e.g., **18**; the degree of delocalization has not been determined) as opposed to a reaction via a diastereoselective S_N2'-like scenario where methanol addition occurs from the β-face of **13a-k**. These observations are fully consistent with the alkyne substituent effects on the stereoselectivity of these heterocycloisomerizations that were observed and rationalized by Schmalz and coworkers using an elegant enantioenriched substrate study.[32]

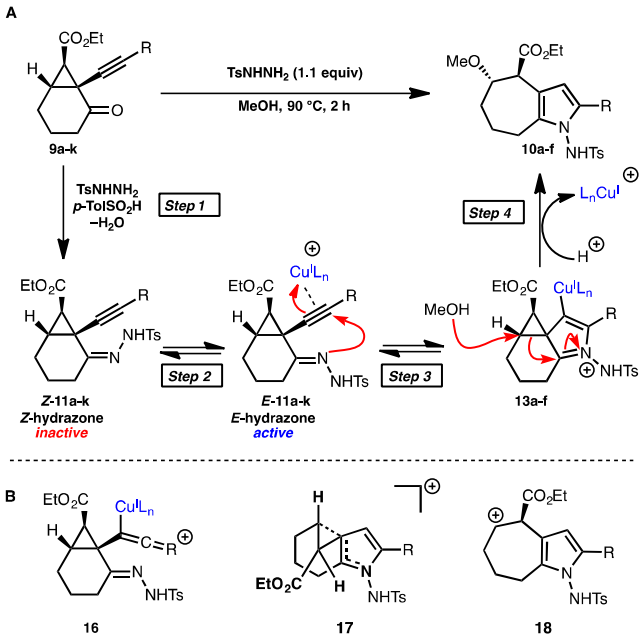

Scheme 2: Mechanistic proposal and rationalization of diastereoselectivity.

CONCLUSION

We report a heterocycloisomerization to form cycloheptane-annulated aminopyrroles facilitated by copper at remarkably low catalyst loadings. These reactions are a 'no-metal added' variant of a related gold(I)-catalyzed cycloisomerization developed by Schmaltz and Zhang for the corresponding furans. Through computational studies, reaction progress monitoring and elemental analysis, we have established that the active catalyst for these reactions is a copper complex present at trace levels. Furthermore, we have demonstrated that both the *E*- and *Z*- hydrazones are formed during this reaction and that, counterintuitively, the *Z*-hydrazone **11** is the more thermodynamically stable hydrazone isomer. We also believe that the thermal decomposition of tosylhydrazide generates diimide and sulfinic acid *in situ*, and these components are critical for the success of the reaction, though we have conclusively shown that the rate-determining step in the reaction has no concentration dependence on the amount of tosylhydrazide added. Computational and kinetic results suggest that enehydrazine **12** is a plausible intermediate in this reaction; however, it is not the species that undergoes cyclization onto the alkyne group and is responsible for isomerization of the hydrazone geometry. With this mechanistic model in hand, we are actively investigating the nature of other "metal-free" cycloisomerization reactions, such as those shown in Figure 1, B, to establish whether trace metal catalysis is involved.

ASSOCIATED CONTENT

Supporting Information

The Supporting Information is available free of charge on the ACS Publications website.

Experimental procedures and spectroscopic data (PDF)
X-ray Crystallographic Data for compound *E*-**11** (cif)
X-ray Crystallographic Data for compound *Z*-**11** (cif)

AUTHOR INFORMATION

Corresponding Authors

* rsarpong@berkeley.edu., djtantillo@ucdavis.edu, jhein@chem.ubc.ca

Present Addresses

†1515 Dickey Dr. Atlanta, GA 30323
††2036 Main Mall, Vancouver, BC V6T 1Z1
†††Internal Medicine, Medicinal Chemistry, Pfizer Worldwide Research & Development, Eastern Point Road, Groton, CT, 06340.

ACKNOWLEDGMENT

The work was supported by the NSF (CAREER 0643264 to RS) NSERC (2016-RGPIN-04613 to JEH) and a Research Scholar Grant from the American Cancer Society (RSG-09-017-01-CDD to RS). In addition, we thank Mettler Toledo Autochem for the donation of a ReactIR-15 (to JEH). We are grateful to the NSF for a graduate fellowship to SMWH and Eli Lilly and Roche for financial support. Computations were supported by the NSF XSEDE program.

REFERENCES

1. For an overview of high-turnover catalyst (HTC), see: Farina, V.; *Adv. Synth. Catal.* **2004**, *346*, 1553 – 1582. For the twelve tenets of green chemistry, see: Anastas, P. T.; Kirchhoff, M. M.; *Acc. Chem. Res.* **2002**, *35,* 686 – 694. For microreview on trace metal catalysis, see: Hierso, J.-C.; Beaupérin, M.; Meunier, P. *Eur. J. Inorg. Chem.* **2007**, *24,* 3767 – 3780. For seminal work on HTC initially using palladacycles, see: Herrmann, W. A.; Brossmer, C.; Öefele, K.; Reisinger, C.-P.; Priermeier, T.; Beller, M.; Fischer, H.; *Angew. Chem. Int. Ed. Engl.* **1995**, *34*, 1844 – 1848. Using adamantlyphosphine based ligands, see: Zapf, A.; Ehrentraut, A.; Beller, M.; *Angew. Chem.* **2000**, *112*, 4315 – 4317; *Angew. Chem. Int. Ed.* **2000**, *39*, 4153 – 4155. For seminal examples of trace palladium catalyst using dialkylbiarylphosphine ligands, see: Wolfe, J. P.; Buchwald, S. L.; *Angew. Chem. Int. Ed.* **1999**, *38*, 2413 - 2416. Wolfe, J. P.; Singer, R. A.; Yang, B. H.; Buchwald, S. L.; *J. Am. Chem. Soc.* **1999**, *121*, 9550- 9561.

2. Littke, A. F.; Fu, G. C. *Angew. Chem. Int. Ed.* **2002**, *41*, 4176 – 4211. Littke, A. F.; Dai, C.; Fu, G. C. *J. Am. Chem. Soc.* **2000**, *122*, 4020 – 4028.
3. Suzuki coupling using Q-Phos Pd catalyst at 0.0005 mol%, see Kataoka, N.; Shelby, Q.; Stambuli, J. P.; Hartwig, J. F.; *J. Org. Chem.* **2002**, *67*, 5554 – 5566. HTC Heck couplings, see Shaughnessy, K. H.; Kim, P.; Hartwig, J. F. *J. Am. Chem. Soc.*, **1999**, *121*, 2123 – 2132.
4. For work on HTC using multidentate phosphines on very electron poor arene, see: Feuerstein, M.; Doucet, H.; Santelli, M.; *Synlett* **2001**, 1458 – 1460.
5. (a) For trace metal catalyzed Suzuki couplings, see: Leadbeater, N. E.; Marco, M. *Angew. Chem. Int. Ed.* **2003**, *42*, 1407 - 1409.; Leadbeater, N. E.; Marco, M. *Org. Lett.*, **2002**, *4*, 2973 - 2976.; Leadbeater, N. E.; Marco, M. *J. Org. Chem.* **2003**, *68*, 5660 - 5667.; Arvela, R. K.; Leadbeater, N. E.; Sangi, M. S.; Williams, V. A.; Grandados, P.; Singer, R. D.; *J. Org. Chem.* **2005**, *70*, 161 - 168. (b) For a review of trace metal contaminants with $FeCl_3$, see Buchwald, S. L.; Bolm, C. *Angew. Chem. Int. Ed*. **2009**, *48*, 5586 – 5587.; Thomé, I; Nijs, A.; Bolm, C.; *Chem. Soc. Rev.* **2012**, *41*, 979 - 987.; Larsson, P.-F.; Correa, A.; Carril, M.; Norrby, P.-O.; Bolm, C. *Angew. Chem. Int. Ed.*, **2009**, *48*, 5691 - 5693.
6. Kirsch, S. *Synthesis* **2008**, 3183–3204.
7. Michelet, V.; Toullec, P. Y.; Genêt, J.-P. *Angew. Chem. Int. Ed.* **2008**, *47*, 4268–4315.
8. Chianese, A. R.; Lee, S. J.; Gagné, M. R. *Angew. Chem. Int. Ed.* **2007**, *46*, 4042–4059.
9. Aubert, C.; Buisine, O.; Malacria, M. *Chem. Rev*. **2002**, *102*, 813–834.
10. Trost, B. M. *Acc. Chem. Res*. **2002**, 35, 695–705.
11. Li, C.-J.; Trost, B. M. *Proc. Natl. Acad. Sci. U. S. A*. **2008**, 105, 13197–13202.
12. a) Bhanu Prasad, B. A.; Yoshimoto, F. K.; Sarpong, R. *J. Am. Chem. Soc*. **2005**, *127*, 12468–12469.; Smith, C. R.; Bunnelle, E. M.; Rhodes, A. J.; Sarpong, R. *Org. Lett*. **2007**, *9*, 1169–1171.; Fisher, E. L.; Wilkerson-Hill, S. M.; Sarpong, R. *J. Am. Chem. Soc*. **2012**, *134*, 9946–9949.
13. Godoi, B.; Schumacher, R. F.; Zeni, G. *Chem. Rev*. **2011**, *111*, 2937–2980.; Gulevich, A. V.; Dudnik, A. S.; Chernyak, N.; Gevorgyan, V. *Chem. Rev.* **2013**, *113*, 3084 - 3213.; Seregin, I. V.; Schammel, A. W.; Gevorgyan, V. *Org. Lett*. **2007**, *9*, 3433–3436.; Li, Z.; Chernyak, D.; Gevorgyan, V. Org. Lett. 2012, 14, 6056–6059.; Chernyak, D.; Gevorgyan, V. *Org. Lett*. **2010**, *12*, 5558–5560.; Seregin, I. V.; Gevorgyan, V. *J. Am. Chem. Soc.* **2006**, *128*, 12050–12051.; Chernyak, D.; Gadamsetty, S. B.; Gevorgyan, V. *Org. Lett*. **2008**, *10*, 2307–2310.; Li, Z.; Chernyak, D.; Gevorgyan, V. *Org. Lett*. **2012**, *14*, 6056–6059.
14. (a) Narayan, A. R. H.; Sarpong, R. *Green Chem*. **2010**, *12*, 1556 - 1559. (b) Heller, S. T.; Kiho, T.; Narayan, A. R. H.; sarpong, R. *Angew. Chem. Int. Ed.* **2013**, *52*, 11120 – 11133.
15. Zhang, J.; Schmalz, H.-G. *Angew. Chem. Int. Ed.* **2006**, *45*, 6704–6707.
16. For the merits of merging synthesis, computation and kinetics, see: (a) Lineberger, W. C.; Borden, W. C. *Phys. Chem. Chem. Phys.* **2011**, *13*, 11792 – 11813. (b) For recent applications to understanding KOtBu mediated reactions, see: Liu, W.-B.; Schuman, D. P.; Yang, Y.-F.; Toutov, A. A.; Liang, Y.; Klare, H. F. T.; Nesnas, N.; Oestreich, M.; Blackmond, D. G.; Virgil, S. C.; Banerjee, S.; Zare, R. N.; Grubbs, R. H.; Houk, K. N.; Stoltz, B. M. *J. Am. Chem. Soc.* **2017**, *139*, 6867 – 6879. (c) Banerjee, S.; Yang, Y.-F.; Jenkins, I. D.; Liang, Y.; Toutov, A. A.; Liu, W.-B.; Schuman, D. P.; Grubbs, R. H.; Stoltz, B. M.; Krenske, E. H.; Houk, K. N.; Zare, R. N. *J. Am. Chem. Soc.* **2017**, *139*, 6880 – 6887.
17. For studies on *E*- and *Z*- hydrazone isomerism, see Hegarty, A. F.; Scott, F. L.; *J. Org. Chem.* **1968**, *753* - 762.; Karabatsos, G. J.; Vane, F. M.; Taller, R. A.; Hsi, N. *J. Am. Chem. Soc.* **1964**, *86*, 3351 – 3357.; Karabatsos, G. J.; Taller, R. A.; Vane, F. M.; *Tetrahedron Lett.* **1964**, 1081 - 1085.; Karabatsos, G. J.; Taller, R. A.; *J. Am. Chem. Soc.* **1963**, *85*, 3624 - 3629.; Karabatsos, G. J.; Shaprio, B. L.; Vane, F. M.; Fleming, J. S.; Ratka, J. S. *J. Am. Chem. Soc.* **1963**, *85*, 2784 - 2788.; Wilson, R. Marshall; Rekers, J. W.; Packard, A. B.; Elder, R. C.; *J. Am. Chem. Soc.* **1980**, *102*, 1633 – 1641.; Adam, W.; Sahin, C.; Schneider, M.; *J. Am. Chem. Soc.* **1995**, *117*, 1695 – 1702. For studies on azomethine imines, see: Gergely, J.; Morgan, J. B.; Overman, L. E.; Bélanger, G.; Hong, F.-T.; Overman, L. E.; Rogers, B. N.; Tellew, J. T.; Trenkle, W. C. *J. Org. Chem.* **2002**, *67*, 7880 - 7883.; Overman, L. E.; Tellew, J. T. *J. Org. Chem.* **1996**, *61*, 8338 – 8340.
18. This value is above the theoretical limit for KIE's that do not involve tunneling for proton transfers, see: Kiefer, P. M.; Hynes, J. T. *J. Phys. Org. Chem*. **2010**, *23*, 632 – 646.
19. Zhao, Y.; Truhlar, D. *Theor. Chem. Acct.* **2008**, *120*, 215 - 241.
20. Gaussian 09, Revision B.01 Frisch, M. J.; Trucks, G. W.; Schlegel, H. B.; Scuseria, G. E.; Robb, M. A.; Cheeseman, J. R.; Scalmani, G.; Barone, V.; Mennucci, B.; Petersson, G. A.; Nakatsuji, H.; Caricato, M.; Li, X.; Hratchian, H. P.; Izmaylov, A. F.; Bloino, J.; Zheng, G.; Sonnenberg, J. L.; Hada, M.; Ehara, M.; Toyota, K.; Fukuda, R.; Hasegawa, J.; Ishida, M.; Nakajima, T.; Honda, Y.; Kitao, O.; Nakai, H.; Vreven, T.; Montgomery, J. A.; Peralta, J. E.; Ogliaro, F.; Bearpark, M.; Heyd, J. J.; Brothers, E.; Kudin, K. N.; Staroverov, V. N.; Kobayashi, R.; Normand, J.; Raghavachari, K.; Rendell, A.; Burant, J. C.; Iyengar, S. S.; Tomasi, J.; Cossi, M.; Rega, N.; Millam, J. M.; Klene, M.; Knox, J. E.; Cross, J. B.; Bakken, V.; Adamo, C.; Jaramillo, J.; Gomperts, R.; Stratmann, R. E.; Yazyev, O.; Austin, A. J.; Cammi, R.; Pomelli, C.; Ochterski, J. W.; Martin, R. L.; Morokuma, K.; Zakrzewski, V. G.; Voth, G. A.; Salvador, P.; Dannenberg, J. J.; Dapprich, S.; Daniels, A. D.; Farkas; Foresman, J. B.; Ortiz, J. V.; Cioslowski, J.; Fox, D. J. Wallingford CT, 2009.
21. Marenich, A. V.; Cramer, C. J.; Truhlar, D. G. *J. Phys. Chem. B* **2009**, *113*, 6378 - 6396.
22. Intrinsic Reaction Coordinate (IRC) calculations were used to connect transition state structures to their local minima, as described in: (a) Gonzalez, C.; Schlegel, H. B. *J. Chem. Phys.* **1991**, *95*, 5853 - 5860. (b) Gonzalez, C.; Schlegel, H. B. *J Chem. Phys.* **1989**, *90*, 2154 - 2161. (c) C. Lee, C.; Yang, W.; Parr, R. G. *Phys Rev. B* **1988**, *37*, 785 - 789. (d) Fukui, K. *Acc. Chem. Res.* **1981**, *14*, 363 – 368.
23. Structural images were created with *Ball & Stick*, see: Ball & Stick 4.0a12, Muller, N.; Faulk, A. *Johannes Kepler University Linz* **2004**.
24. Predicted KIE values were computed using the Bigeleisen and Mayer method, as implemented in *Quiver*. (a) Bigeleisen, J.; Mayer, M. G. *J. Chem. Phys.* **1947**, *15*, 261-267. (b) Saunders, W.; Laidig, K. E.; Wolfsberg, M. *J. Am. Chem. Soc.* **1999**, *111*, 8989-8994. (c) A modified version of *Quiver* provided by Prof. Daniel Singleton (Texas A&M) was utilized.
25. Phinyocheep, P.; Pasiri, S.; Tavichai, O. *J. Appl. Polym. Sci.* **2003**, *87,* 76–82.; Podešva, J.; Holler, P. J. Appl. *Polym. Sci.* **1999**, *74,* 3203–3213.; Samran, J.; Phinyocheep, P.; Daniel, P.; Kittipoom, S. *J. Appl. Polym. Sci.* **2005**, *95,* 16–27.
26. (a) Dunn, A. L.; Landis, C. R. *Magn. Reson. Chem.* **2017**, *55*, 329–336. (b) Foley, D. A.; Bez, E.; Codina, A.; Colson, K. L.; Fey, M.; Krull, R.; Piroli, D.; Zell, M. T.; Marquez, B. L. *Anal. Chem*. **2014**, *86*, 12008–12013.
27. (a) Chung, R.; Hein, J. E. *Top. Catal*. **2017**, *137*, 1–15. (b) Theron, R.; Wu, Y.; Yunker, L. P. E.; Hesketh, A. V.; Pernik, I.; Weller, A. S.; McIndoe, J. S. *ACS Catal*. **2016**, *6*, 6911–6917. (c) Foley, D. A.; Doecke, C. W.; Buser, J. Y.; Merritt, J. M.; Murphy, L.; Kissane, M.; Collins, S. G.; Maguire, A. R.; Kaerner, A. *J. Org. Chem*. **2011**, *76*, 9630–9640.
28. (a) Rougeot, C.; Situ, H.; Cao, B. H.; Vlachos, V.; Hein, J. E. *React. Chem. Eng.* **2017**, *2* (2), 226–231. (b) Malig, T. C.; Koenig, J. D. B.; Situ, H.; Chehal, N. K.; Hultin, P. G.; Hein, J. E. *React. Chem. Eng.* **2017**, *2* (3), 309–314.
29. X-Ray structures were visualized with: Legault, CYL *view* 1.0b; Universitè de Sherbrooke: Quebec, Canada, 2009; http://www.cylview.org.

30. Hay, P. J.; Wadt, W. R. *J. Chem. Phys.* **1985**, *82*, 270-283.
31. Jones, R. A.; Marriott, M. T. P.; Rosenthal, W. P.; Sepulveda Arques, J. *J. Org. Chem.* **1980**, *45*, 4515–4519; Hosmane, R. S.; Hiremath, S. P.; Schneller, S. W.; *J. Chem. Soc. Perkin Trans. 1* **1973**, 2450 – 2453.
32. Labsch, S.; Ye, S.; Adler, A.; Neudörfl, J.-M.; Schmalz, H.-G. *Tetrahedron Asymm.* **2010**, *21*, 1745–1751.

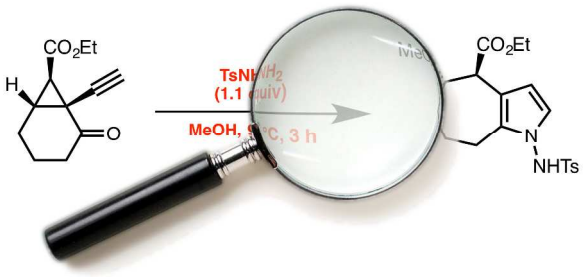
CO2Et
H
O
TsNHNH2
(1.1 equiv)
MeOH, 0 °C, 3 h
MS
CO2Et
N
NHTs